Photochemical & Photobiological Sciences
https://doi.org/10.1007/s43630-026-00866-4

RESEARCH

Water-soluble phthalocyanines with non-peripheral naphthoxy-sulfonate substituents: computational docking, biological and sono-photochemical investigations

Armağan Günsel[1] · Ceren Can Karanlık[2,9] · Parham Taslimi[3] · Hilal Günsel[4] · Tugba Taskin-Tok[5,6,7] · Ahmet T. Bilgiçli[1] · Eda Mehtap Özden[8] · İlhami Gülçin[8] · Ali Erdoğmuş[2,9] · M. Nilüfer Yarasir[1]

Received: 7 October 2025 / Accepted: 26 January 2026
© The Author(s) 2026

Abstract

This study reports the synthesis of a novel ligand, sodium 6-(2,3-dicyanophenoxy)naphthalene-2-sulfonate **(1)**, and the corresponding non-peripherally substituted metallophthalocyanines (MPcs) [M = Zn(II) **(2)**, Ga(III) **(3)**; X = Cl, In(III) **(4)**; X = Cl]. These compounds were functionalized with 6-naphthoxy-2-sulfonic acid sodium salt groups. Given the limitations of conventional photodynamic therapy (PDT), we investigated the potential of sonophotodynamic therapy (SPDT), a dual-modality approach combining light and ultrasound, to enhance singlet oxygen ($^1O_2$) production. Among the synthesized metallophthalocyanines, the zinc(II) complex **(2)** shows the highest $^1O_2$ production in both organic and aqueous media under both photochemical and sonophotochemical conditions, showing promise for SPDT applications. Furthermore, the inhibitory effects of these complexes on acetylcholinesterase (AChE) and human carbonic anhydrase isoenzymes (hCA I and II), important targets for Alzheimer's disease, glaucoma, and epilepsy, were evaluated. The compounds showed strong inhibition with K_i values ranging from 130.31 ± 6.18 to 157.47 ± 9.37 µM for hCA I (compared to AZA: 177.41 ± 11.40 µM), 99.18 ± 8.13 to 106.72 ± 8.50 µM for hCA II (compared to AZA: 143.51 ± 9.94 µM) and 0.31 ± 0.03 to 1.21 ± 0.01 µM for AChE (compared to TAC: 1.24 ± 0.21 µM). Molecular docking revealed strong binding affinities: In(III)-Pc **(4)** showed the highest affinity for AChE (BE: -26.96 kcal/mol), while Ga(III)-Pc **(3)** preferentially bound to hCA I and II (BE: -13.90 and −15.39 kcal/mol, respectively). These findings position the synthesized MPcs as multifunctional agents for SPDT and enzyme-targeted therapies.

Keywords Phthalocyanine · Synthesis · Singlet oxygen · Bioactivity · In silico study

✉ Armağan Günsel
agunsel@sakarya.edu.tr

[1] Department of Chemistry, Faculty of Science, Sakarya University, Serdivan, Sakarya, Türkiye

[2] Department of Chemistry, Faculty of Arts and Sciences, Yıldız Technical University, Esenler, Istanbul, Türkiye

[3] Faculty of Science, Department of Biotechnology, Bartin University, 74110 Bartin, Türkiye

[4] Department of Engineering Fundamental Sciences, Faculty of Technology, Sakarya University of Applied Sciences, Serdivan, Sakarya, Türkiye

[5] Faculty of Arts and Sciences, Department of Chemistry, Gaziantep University, Gaziantep, Türkiye

[6] Institute of Health Sciences, Department of Bioinformatics and Computational Biology, Gaziantep University, Gaziantep, Türkiye

[7] Gaziantep University, Ulug Bey High Technology Application and Research Center (ULUTEM), Gaziantep, Türkiye

[8] Faculty of Science, Department of Chemistry, Atatürk University, 25240 Erzurum, Türkiye

[9] Health Biotechnology Joint Research and Application Center of Excellence, 34220 Istanbul, Türkiye

Published online: 16 February 2026

1 Introduction

Phthalocyanines are versatile compounds with a rich chemistry and wide-ranging applications [1]. Photodynamic therapy (PDT) is indeed one of the most significant and impactful applications of phthalocyanines. This advanced medical treatment leverages the unique properties of phthalocyanines to treat various medical conditions, primarily cancer [2–5]. Phthalocyanines act as photosensitizers in PDT. Especially, certain metallophthalocyanines (e.g., zinc phthalocyanine, gallium phthalocyanine) are used as photosensitizers in photodynamic therapy [6]. When exposed to a specific wavelength of light, these compounds become excited and transfer energy to surrounding molecular oxygen, converting it into reactive oxygen species (ROS), such as singlet oxygen. The generated ROS are highly reactive and can cause significant damage to cellular structures, including membranes, proteins, and DNA. This leads to cell death, primarily through apoptosis (programmed cell death) or necrosis. The light used in PDT can be precisely directed at the tumor, minimizing damage to surrounding healthy tissues. Beyond their photophysical and photochemical versatility, metallophthalocyanines have attracted interest as multifunctional macrocyclic platforms capable of interacting with a variety of biological targets. This study investigated the inhibitory effects of synthesized Zn(II), Ga(III), and In(III) phthalocyanines on acetylcholinesterase (AChE) and human carbonic anhydrase isoenzymes (hCA I and II). The aim of this study is not to propose these compounds as direct therapeutic agents, but rather to explore their potential as enzyme-responsive scaffolds relevant to neurodegenerative and metabolic disorders. This information may guide the design of photoactive molecular probes or multifunctional photosensitizers that can combine diagnostic and therapeutic functions within the same molecular framework. Additionally, phthalocyanines can be engineered to accumulate preferentially in cancer cells, enhancing the specificity and efficacy of the treatment [7, 8]. Sono-photodynamic therapy (SPDT) has emerged as an advanced and potentially more effective variant of photodynamic therapy (PDT). In addition to light, SPDT uses ultrasound waves to activate the photosensitizer. Ultrasound can penetrate deeper into tissues than light, enabling the treatment of tumors located deep within the body. The ultrasound waves induce cavitation and sonochemical reactions, which further generate ROS and enhance the therapeutic effect [9–13]. Functional groups such as sodium sulfonate are critical for enhancing the performance of phthalocyanines in photodynamic therapy. Sodium sulfonate groups are highly hydrophilic, which greatly enhances the water solubility of phthalocyanines. This is crucial because many unmodified phthalocyanines are poorly soluble in aqueous environments, limiting their use in biological systems. These modifications make sulfonated phthalocyanines highly effective photosensitizers for PDT/SPDT, contributing to more successful and targeted cancer treatments [14–17].

The metalloenzyme superfamily known as human carbonic anhydrases (hCAs), or carbonate dehydratases, is present in all living things and has a Zn^{2+} ion at its active site. Their primary role in metabolism is to catalyze the reversible form of bicarbonates from carbon dioxide. Numerous physiological and pathological activities, such as ion and gas exchange, pH regulation, photosynthesis, calcification, and multiple biosynthetic pathways like gluconeogenesis, lipogenesis, and ureagenesis, depend vitally on CAs [18, 19]. Some carbonic anhydrases, such as CA I, II, III, VII, and XIII, are cytosolic, whereas CA IV, IX, XII, XIV, and XV are membrane-bound, out of the 16 isoenzymes. The catalytic Zn^{2+} ion in CA isoenzymes is the target of carbonic anhydrase inhibitors (CAIs), which lower their activity. In individuals with glaucoma, CA II inhibitors can reduce intraocular pressure because it regulates the amounts of bicarbonate in the eye. Inhibitors of CA II are being investigated as complementary therapy in the treatment of cancer since it is also present in a variety of malignancies, such as renal, gastric, brain, and pancreatic tumors [20, 21]. The importance of these compounds in this study for additional optimization for pharmacological profiling and the development of therapeutic medicines against hCA I and II is thus clarified by the combination of the two studies, the enzyme inhibition assay and the molecular docking research. Additionally, this work offers information for further investigation into the production of novel compounds that inhibit hCA I and II for medicinal purposes. A slowly progressing neurodegenerative disease, Alzheimer's disease (AD) is the most common type of dementia. It is identified by the buildup of amyloid-beta (Aβ) peptide in the most affected region of the brain. According to estimates, 6.9 million adults 65 and older suffer from AD. But without new pharmacological approaches to prevent or cure AD, the number of people affected might rise to 13.8 million by 2060. As with the initial findings, the "cholinergic hypothesis" of AD was developed as a result of the anomalies in acetylcholine metabolism found in AD brains [22, 23]. In accordance with this notion, the hallmark of AD patients' basal forebrain appears to be cholinergic neuron depletion coupled with tau and Aβ buildup. Acetylcholine (ACh), an excitatory neurotransmitter, plays a crucial role in memory, learning, and other higher-functioning behaviors. The central cholinergic nerve system can change the amount of ACh by regulating its production and release. Choline acetyltransferase in presynaptic neurons converts choline and acetyl coenzyme A into ACh, which is then released into synaptic gaps to control cognitive functions [24, 25]. At the synaptic cleft, acetylcholinesterase (AChE)

rapidly hydrolyzes ACh to create acetate and choline, which are then recycled into the presynaptic nerve terminal to sustain the ACh level. However, the overproduction of AChE stops ACh-mediated neurotransmission. Low amounts of ACh can impair memory in AD patients. Two drug types have been licensed by the FDA to treat AD: AChE inhibitors (donepezil, galantamine, and rivastigmine) and NMDA receptor blockers (memantine) [26, 27].

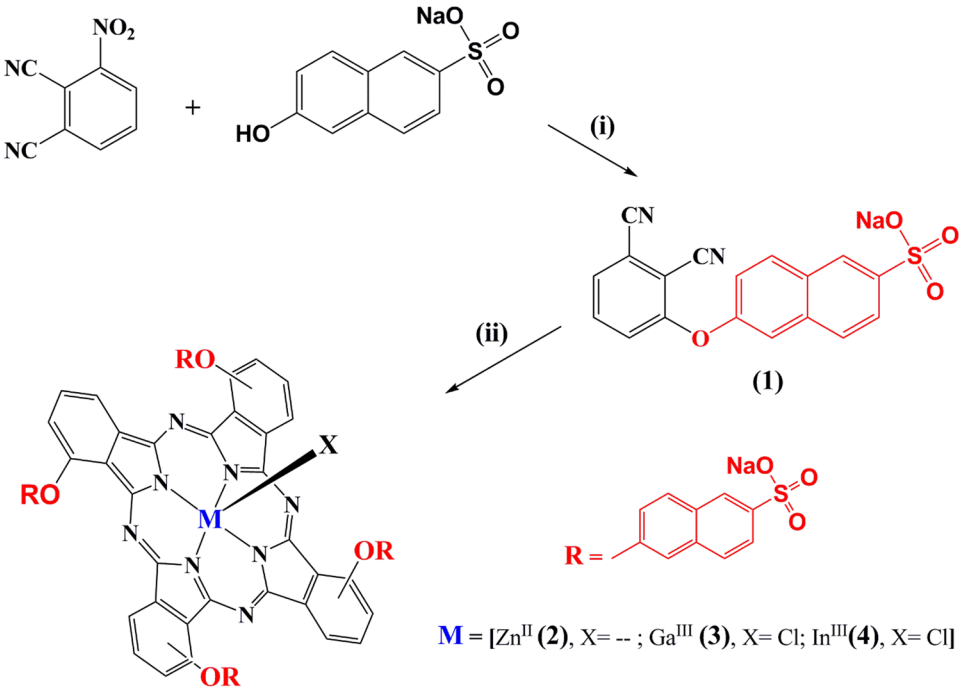
This study presents the synthesis and characterization of a novel ligand, *sodium 6-(2,3-dicyanophenoxy) naphthalene-2-sulfonate* **(1)**, along with its newly prepared tetra-α-substituted phthalocyanine derivatives containing zinc(II) **(2)**, gallium(III) chloride **(3)**, and indium(III) chloride **(4)** as central metal ions. First goal of this study is to show the important of irradiation method on generation of singlet oxygen. In the photochemical method, the synthesized compounds **(2–4)** were excited with light, while in the sonophotochemical method, both ultrasound and light were used as stimulants and singlet oxygen efficiency were evaluated comparatively. Among them, the Zn(II) complex **(2)** demonstrated notably high singlet oxygen quantum yields (ΦΔ = 0.81 in DMSO), highlighting the success of the design strategy. This approach offers a promising alternative to conventional photosensitizers, particularly in addressing the limitations posed by hypoxic tumor environments. The prominent structural and functional advantages of these novel compounds include: "Efficient light absorption within the therapeutic window, High activity in both aqueous and organic media, Dual activation capability via light and ultrasound, Compatibility with hypoxic tumor microenvironments, Enhanced biocompatibility and photochemical stability". The second goal of this study is to examine the inhibitory capabilities of certain metabolic enzymes; to this end, metallophthalocyanines have been developed. In addition to their high solubility, the synthesized metallophthalocyanine complexes were found to have anticholinergic and antiepileptic properties. Additionally, we use molecular docking studies to examine the activity of the complexes under study with the metabolic enzymes described. Also, in silico applications are applied to gain a deeper insights of the molecular-level interactions of these compounds.

2 Results and discussion

2.1 Synthesis and characterization of the compounds

The synthetic pathway for the preparation of the ligand "sodium 6-(2,3-dicyanophenoxy)naphthalene-2-sulfonate" **(1)** and its non-peripherally substituted zinc **(2)**, gallium **(3)**, and indium **(4)** phthalocyanine derivatives is illustrated in Scheme 1. The cyclotetramerization of compound **(1)** with anhydrous metal salts [$Zn(CH_3COO)_2$, $GaCl_3$, and $InCl_3$] was carried out in dry DMSO at 180 °C, affording the non-peripherally substituted phthalocyanines **(2–4)** bearing (6-naphthoxy-2-sulfonic acid sodium salt) units.

The formation and electronic features of the phthalocyanines were first verified by UV-Vis spectroscopy. As expected, the spectra of compounds **(2–4)** displayed intense Q-bands characteristic of π–π* transitions, observed at 695 nm for **(2)**, 711 nm for **(3)**, and 708 nm for **(4)** in DMSO



Scheme 1 Synthetic route of *1(4), 8(11), 15(18), 22(25)-tetrakis (6-naphthoxy-2-sulfonic acid sodium salt) metallophthalocyanines*; (M = Zn(II), Ga(III) and In(III)]. Reagents and conditions; **(i)** Na_2CO_3, DMSO, rt, 3 days, **(ii)** Dimethyl sulfoxide (DMSO), 1,8-diazabicyclo[5.4.0]undec-7-ene (DBU) reflux, 8 h

(Fig. 1). Measurements conducted in aqueous media containing Triton X-100 revealed no significant aggregation, with Q-band absorptions detected at 694 nm for **(2)**, 722 nm for **(3)** (Fig. S1) and 718 nm for **(4)**, respectively. The presence of distinct Q and B bands thus confirmed the successful formation of the phthalocyanine macrocycles [28].

FT-IR spectroscopy further supported the structural assignment. Compound **(1)** exhibited characteristic absorptions at 3055, 2228, 1352, 1150, 761, and 656 cm^{-1}, attributable to aromatic C-H stretching, C ≡ N, strong asymmetric and symmetric S = O stretching, C-S stretching, and S-O stretching vibrations, respectively [29, 30]. Importantly, the disappearance of the C ≡ N band in the spectra of **(2–4)** indicated successful cyclotetramerization. Apart from minor shifts, the overall spectral features of the phthalocyanines closely resembled those of the precursor **(1)**.

NMR spectroscopy provided additional confirmation. In the ^{1}H-NMR spectrum of compound **(1)**, aromatic resonances were observed between 8.20 and 7.27 ppm (Fig. S2), while its ^{13}C-NMR spectrum in dmso exhibited signals at δ = 159.97, 153.76, 144.39, 135.64, 133.76, 132.49, 130.64, 129.43, 126.58, 125.02, 123.13, 122.83, 118.49, 116.92, 116.33, 114.08, 110.71 and 105.99 ppm (Fig. S3). In contrast, the ^{1}H-NMR spectra of phthalocyanines **(2–4)** displayed broad resonances between 8.65 and 7.12 ppm, consistent with aggregation tendencies and the presence of isomeric mixtures [31, 32].

MALDI-TOF mass spectrometry provided final confirmation of the target compounds. For ligand **(1)**, signals were detected at m/z 328.065 $[M–2Na+2\ H]^+$, 356.269 $[M–K + Na]^+$, 373.039 $[M + H]^+$, 394.492 $[M + Na–H]^+$, and 410.483 $[M + K–H]^+$ (Fig. S4). Compound **(2)** displayed peaks at m/z 1530.662 $[M–Na–H]^+$, 1592.023 $[M–Na–K]^+$, 1585.938 $[M+3Na–K + H]^+$, 1620.951 $[M+3Na–3\ H]^+$, and 1661.300 $[M+3Na + K–H]^+$. For compound **(3)**, signals appeared at m/z 1536.051 $[M–Na–Cl]^+$, 1595.623 $[M + H]^+$, and 1664.462 $[M+3Na + H]^+$ (Fig. S5). Finally, compound **(4)** exhibited peaks at m/z 1580.142 $[M–Na–Cl]^+$, 1640.521 $[M + H]^+$, and 1686.332 $[M+2Na + H]^+$. The presence of potassium-related adducts was attributed to trace impurities, which are known to stabilize such species in the gas phase [33, 34].

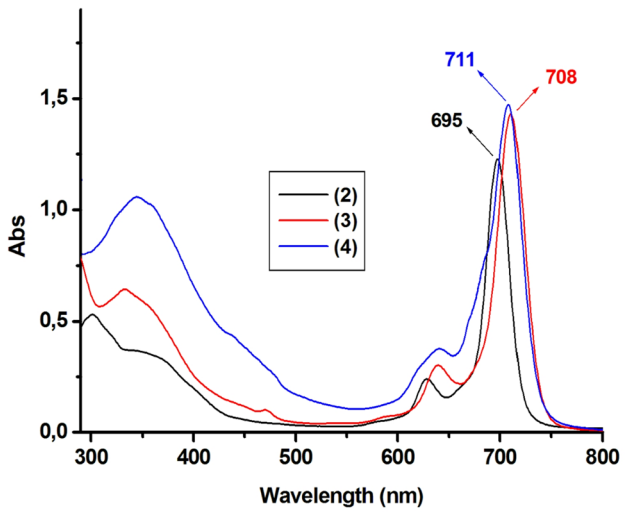


Fig. 1 UV-Vis spectra of the phthalocyanines **(2–4)** ~ $14.0 \times 10^{6-}$ M in DMSO

2.2 Aggregation studies

The control of aggregation in phthalocyanines is a key factor in determining their optical and functional performance. Variables such as concentration, solvent polarity, substituents, and the central metal ion can be strategically modified to modulate aggregation behavior, thereby tuning the electronic and photophysical properties of these macrocycles. In biomedical contexts, particularly in photodynamic therapy, aggregation strongly influences the quantum yield of singlet oxygen generation. Structural modification through steric substituents, solvent selection, and the use of additives or surfactants are widely employed strategies to regulate aggregation [35–37].

To evaluate these effects, the UV–Vis absorption spectra of phthalocyanines **(2–4)** were recorded in DMSO across the concentration ranges of $8.0 \times 10^{-6} – 1.0 \times 10^{-6}$ M (Fig. S6) and in water between $16.0 \times 10^{-6} – 1.0 \times 10^{-6}$ M (Fig. S7). In DMSO, the absorption maxima of the Q-band remained essentially unchanged with increasing concentration, and the molar extinction coefficients were nearly constant. This result confirmed that compounds **(2–4)** retained a monomeric form and followed the Beer–Lambert law, without evidence of H- or J-type aggregation [38, 39].

In contrast, spectra obtained in aqueous solution revealed a clear splitting of the Q-band into two distinct components, indicative of aggregate formation through face-to-face stacking of the phthalocyanine rings. The appearance of blue-shifted higher-energy bands reflected strong excitonic interactions between adjacent macrocycles [40–42]. To suppress aggregation, the compounds were subsequently dissolved in water containing Triton X-100. Under these conditions, monomeric absorption features were restored, with red-shifted Q-band maxima at 694 nm for **(2)**, 722 nm for **(3)**, and 718 nm for **(4)**. The corresponding blue-shifted bands at 646 nm for **(2)**, 672 nm for **(3)**, and 680 nm for **(4)** were attributed to aggregated species. These findings highlight the strong solvent- and environment-dependent aggregation behavior of phthalocyanines **(2–4)**, which is a critical consideration for their practical applications.

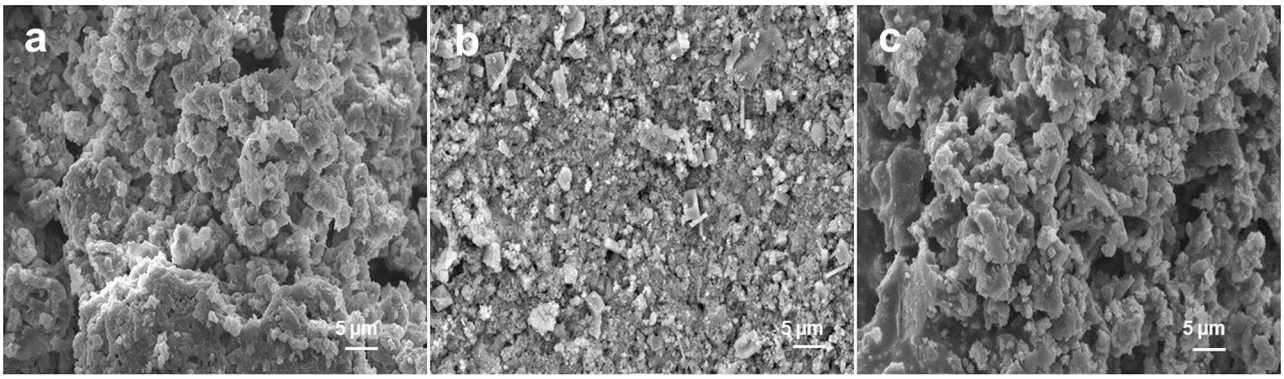


Fig. 2 The SEM images taken from **a** ZnPc **(2)**, **b** GaClPc **(3)**, and **c** InClPc **(4)**

Table 1 Photochemical and sonophotochemical features of Pcs **(2–4)**

Pcs	$\phi_{\Delta(\mathrm{PDT})}$ (DMSO/H_2O)	$\phi_{\Delta(\mathrm{SPDT})}$	$\phi_d\left(10^{-4}\right)$
(2)	0.81 / 0.18	1.23	9.0
(3)	0.68/ 0.17	1.02	6.1
(4)	0.80 / 0.22	1.19	0.3

2.3 Microscopic analysis

The surface morphologies of the synthesized ZnPc **(2)**, GaClPc **(3)**, and InClPc **(4)** samples were examined using a JEOL JSM-6060LV Scanning Electron Microscope (SEM) operated at 15 kV. Representative micrographs of these samples, captured under identical magnification conditions, are presented in Fig. 2a–c. These images provide a comparative visual assessment of the surface characteristics and particle morphologies of the phthalocyanine complexes.

All samples exhibited generally spherical or aggregated morphologies, indicating a certain uniformity in the structural formation process. However, noticeable differences in particle aggregation, porosity, and size distribution were observed depending on the central metal ion. As shown in Fig. 2a, ZnPc **(2)** displayed a rough and porous surface composed of interconnected clusters and plate-like aggregates. GaClPc **(3)** (Fig. 2b) presented a more compact and densely packed morphology with smaller and more uniform particles, while InClPc **(4)** (Fig. 2c) showed an intermediate morphology with moderate surface roughness and partial aggregation.

2.4 Determination of singlet oxygen formation by using photochemical and sonophotochemical methods

The effectiveness of PDT and SPDT applications, which are alternative approaches to cancer treatment, is based on the effectiveness of the sensitizer in producing singlet oxygen. For this reason, evaluating the effectiveness of the sensitizer both photochemically and sonophotochemically is important to form the basis of clinical studies. In this study, the sonophotosensitizer's effectiveness in producing singlet oxygen was assessed by two different methods exposing it to light alone (photochemically) and to both light and sound (sonophotochemically). To evaluate the photochemical potential of Pcs **(2–4)**, the Pcs solution with DPBF were irradiated to specific light for 10-second intervals. Photochemical potential of the compounds was studied in both DMSO and H_2O. To evaluate the sonophotochemical potential, the test solutions were subjected to both ultrasound (35 kHz) and light for 10-second intervals. The change in absorbance of DPBF /ADMA at 417 / 378 nm was monitored using a UV-Vis spectrophotometer. All calculated data are listed in Table 1 and related spectrum are shown in Fig. S8 for **(2)**, Fig S9 for **(4)** and Figs. 3 and 4 for **(3)**. The singlet oxygen values in DMSO higher than H_2O. This is caused by better solubility of oxygen in organic solvent than water [43]. The singlet oxygen quantum yield of all phthalocyanine is higher than unsubstituted ZnPc in both photochemical and sonophotochemical methods in DMSO. When compared with similar structures in the literature [44, 45]. It was observed that the Pcs **(2–4)** have higher capacity of production of singlet oxygen. Also, the phthalocyanine **(2)** photochemically produced higher singlet oxygen compared to other water-soluble Pc derivatives in literature [46–49]. Also, to show the effect of sonochemical methods on DPBF quencher, the measurements only DPBF were used and were irradiated by both sonochemical and sono-photochemical studies. The DPBF absorbances did not change after the irradiation of both sonochemical and sono-photochemical as expected (see in Fig. S10).

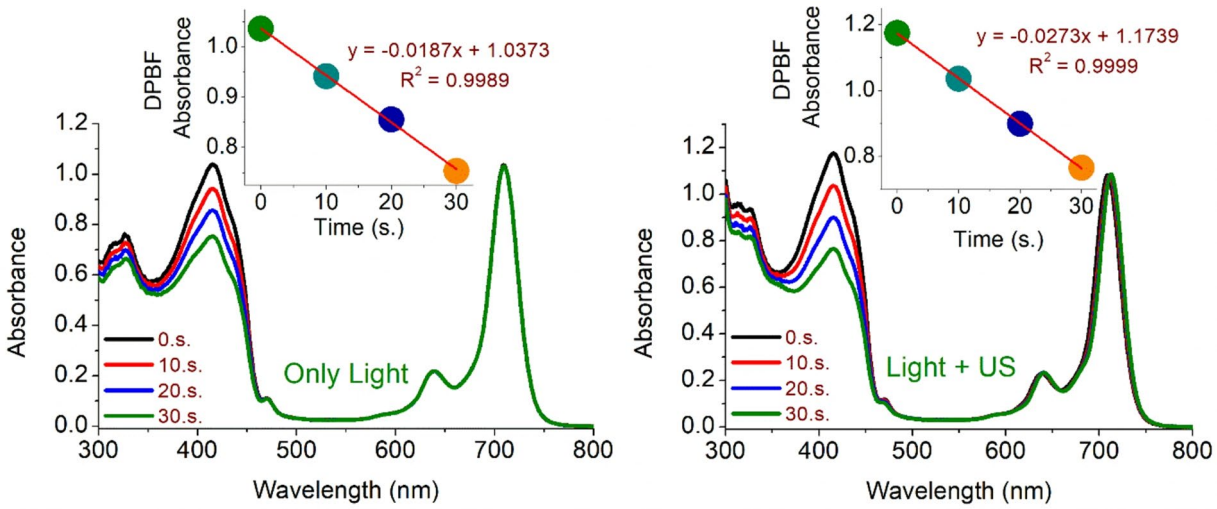


Fig. 3 Typical spectra for the determination of the singlet oxygen quantum yield of GaClPc **(3)** in the photochemical /sonophotochemical study in DMSO

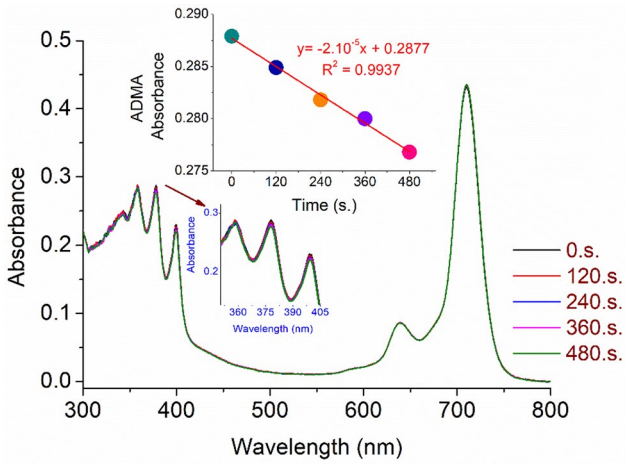


Fig. 4 Typical spectra for the determination of the singlet oxygen quantum yield of GaClPc **(3)** in the photochemical study in H_2O

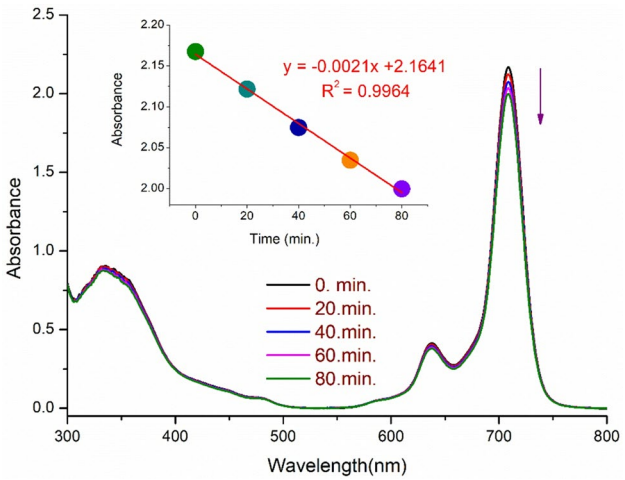


Fig. 5 Typical spectra for the determination of photodegradation quantum yield of GaClPc **(3)** in DMSO

2.5 Determination of photodegradation quantum yields

Photodegradation quantum yield indicates the stability of the photosensitizer under the employed light dose. Since a specific wavelength of light is used to activate the PS in both PDT and SPDT applications, the stability of the sensitizer within this wavelength range is crucial for effective singlet oxygen production and maintaining the drug dose. Therefore, this part of the study focused on determining the photostability of phthalocyanines **(2–4)** in DMSO by monitoring the decrease in the intensity of the absorption band every 20 min under light irradiation. Calculated result showed that indium phthalocyanine **(4)** showing lower stability under light compared to zinc **(2)** and gallium phthalocyanine **(3)**. The photodegradation quantum yield values are listed in Table 1 and the obtained spectra are shown in Fig. S11 and S12 for **(2,4)** and Fig. 5 for **(3)**.

2.6 Biological study

The AChE and two pharmacologically significant hCAs, the cytosolic hCA I and II, were examined in relation to the target derivatives **(2–4)**. Table 2 present the enzyme inhibition constants (KI) and IC50 values. The aromatic/heterocyclic sulfonamide or sulfamate families include the majority of the powerful CAIs that have been studied thus far, while compounds with additional zinc-binding groups have also been studied. In fact, these derivatives participate in a variety of polar and hydrophobic interactions with the cavity's amino acid residues in addition to directly binding to the catalytically important Zn(II) ion of the enzyme active site

Table 2 The enzyme inhibition results of novel complexes against AChE, BChE and α-glycosidase (α-Gly) enzymes

Compounds	IC_{50} (μM)						Ki (μM)		
	hCA I	r^2	hCA II	r^2	AChE	r^2	hCA I	hCA II	AChE
(2)	129.70	0.983	86.15	0.987	0.95	0.983	157.47 ± 9.37	101.40 ± 7.09	0.68 ± 0.05
(3)	110.01	0.993	80.90	0.961	1.47	0.955	130.31 ± 6.18	99.18 ± 8.13	1.21 ± 0.01
(4)	135.76	0.967	96.37	0.995	0.38	0.990	145.60 ± 9.16	106.72 ± 8.50	0.31 ± 0.03
AZA	162.58	0.957	137.81	0.930	-	-	177.41 ± 11.40	143.51 ± 9.94	-
TAC	-	-			1.40	0.971	-	-	1.24 ± 0.21

via the deprotonated sulfonamide/sulfamate moiety. Clinically employed sulfonamide/sulfamate CAIs often exhibit low nanomolar potencies against physiologically significant isozymes, including CA I, II, V, and IX [49, 50].

The hCA I isoenzyme was inhibited by novel metallophthalocyanine compounds **(2**, **3** and **4)**, with IC50 values ranging from 110.01 to 135.76 μM and Ki values between 130.31 ± 6.18 and 157.47 ± 9.37 μM. Specifically, compound **(3)** showed the strongest hCA I inhibitory impact with a KI of 130.31 ± 6.18 μM for *22(25)-tetrakis (6-naphthoxy-2-sulfonic acid sodium salt) phthalocyninato gallium (III) chloride* ***(3)***, medium followed by compound **(4)** with a KI of 145.60 ± 9.16 μM and compound **(2)** with a KI of 157.47 ± 9.37 μM. Compared to the conventional compound AZA, compound **(3)** was roughly 1.5 times more effective, while compound **(2)** was 1.2 times more effective. Every compounds under investigation exhibited superior inhibition compared to the reference compound, AZA (KI: 177.41 ± 11.40 μM). In a similar study conducted by Güzel et al. [51]. For the first time, 3-(2-(5-amino-4-(4-bromophenyl)-3-methyl-1H-pyrazol-1-yl)ethoxy)phthalonitrile (2) and its nitrogen-containing non-peripheral phthalocyanine derivatives (3 and 4) were prepared and their inhibitory properties of the carbonic anhydrase and paraoxonase enzymes were evaluated. FT-IR, ^{1}H-NMR, ^{13}C-NMR, mass, and UV-vis spectroscopy have all been used to clarify the novel phthalonitrile and its phthalocyanine precursors. The findings showed that all of the synthetic compounds had a modest inhibitory effect on the enzymes paraoxonase and carbonic anhydrase. The compounds that were determined to be the most active were compound (1) for hCA II (Ki: 13.62 μ M), compound (3) for hCA I (Ki: 22.52 μM), and compound (4) for PON (Ki: 0.14 μ M).

Table 2 displays the evaluation of the hCA II enzyme inhibition levels. For hCA II, IC50 values fall between 80.90 and 96.37 μM, while KI values fall between 99.18 and 106.72 μM. The compound with the strongest inhibitory effect on hCA II was compound **(3)**. AZA (KI: 143.51 ± 9.94 μM) > **(4)** (KI: 106.72 ± 8.50 μM) > **(2)** (KI: 101.40 ± 7.09 μM) > **(3)** (KI: 99.18 ± 8.13 μM) was the order of potency for hCA II. Furthermore, the hCA II enzyme was more inhibited by these synthetic compounds than hCA I. The degree of inhibition varies between 1.2 and 1.5 times when the chemicals are compared to one another in both enzymes. In another similar study conducted by Çakır and Arslan [52]; They created new silicon(IV)phthalocyanines (SiPcs) for the first time and searched in vitro for important molecular targets. These SiPcs contained 4-hydroxypyridine (1a), N-(2-hydroxyethyl)succinimide (2a), and N-(2-hydroxyethyl)phthalimide (3a) at their axial positions. Several spectroscopic techniques were used to validate the characterization of novel substances. Axially disubstituted silicon phthalocyanines were also tested for their ability to inhibit cholinesterase (AChE and BChE, which are linked to Alzheimer's disease) and carbonic anhydrase isoforms hCA I, II (cytosolic, ubiquitous isozymes), and IX (transmembrane, cancerassociated isozyme). All of the produced compounds showed significant inhibitory effects against these five esterase enzymes, with IC50 values ranging from 49.51 to 231.05 nM. The strongest inhibitory activity against hCA I, AChE, and BChE was demonstrated by 3a out of the three silicon(IV)phthalocyanines. Additionally, 1a showed that hCA II and hCA IX were most effectively inhibited.

Inhibiting acetylcholinesterase (AChE), the enzyme responsible for breaking down acetylcholine, is seen to be a promising treatment approach for neurological conditions such myasthenia gravis, senile dementia, Alzheimer's disease, and ataxia [53]. TAC was used as a reference inhibitor, and the AChE inhibitory ability of synthesized metallophthalocyanine compounds **(2–4)** was evaluated using Ellman's technique. For AChE, the IC50 and KI values fall between 0.38 and 1.47 μM and 0.31 and 1.21 μM, respectively. When compared to TAC (Ki = 1.24 ± 0.21 μM), two of the three chemicals examined, **(3)** and **(1)**, were shown to be strong inhibitors of AChE, with KI values of 0.31 ± 0.03 and 0.68 ± 0.05 μM, respectively. In another study by Güzel et al.; [54]. They reported for the first time the synthesis, aggregation behavior, and analysis of the inhibitory properties of the enzymes cholinesterase and carbonic anhydrase of non-peripherally (4-isopropylbenzyl)oxy-substituted phthalocyanines (4–6). UV-Vis (ultraviolet-visible), FT-IR (Fourier transform infrared spectroscopy), NMR (nuclear magnetic resonance), and MALDI-TOF (matrix-assisted laser desorption/ionization time-of-flight) mass spectrometry were used to determine the chemical structures of these novel phthalocyanines. The phthalocyanines'

Q-band redshift and exceptional solubility are enhanced by the substitution of 4-isopropylbenzyl)oxy groups. Additionally, these compounds were examined in relation to a number of enzymes, including acetylcholinesterase, human carbonic anhydrase I and II isoforms, and butyrylcholinesterase. Ki values for the phthalocyanine complexes were in ranging of 478.13 ± 57.25–887.25 ± 101.20 µM against hCA I, 525.16 ± 45.87–921.14 ± 81.25 µM against hCA II, 68.33 ± 9.13–201.15 ± 35.86 µM against AChE, and 86.25 ± 13.65–237.54 24.7 µM against BChE, respectively. In a different investigation, Tekin and Arslan's article [55] examined the anti-AD properties of previously synthesized tetra-chalcone-substituted metallophthalocyanines (MPcs) with Ni(II), Zn(II), Co(II), and Cu(II) in the inner core activities. The original Ellman's colorimetric method was used to assess the MPcs' ability to inhibit acetylcholinesterase (AChE) and butyrylcholinesterase (BChE). All substances exhibited inhibitory actions against these two cholinesterase enzymes, with IC50 values ranging from 2.865 to 3.372 µM against BChE and 1.243–2.369 µM against AChE. CuPcs (2) had the highest inhibitory activity against AChE among the four MPcs. Additionally, ZnPcs (3) demonstrated the best BChE inhibition.

2.7 Docking results

According to the in vitro analysis results, docking calculations deeply explain the internal structure of the biological events that occur with the target enzymes AChE, hCA I, and hCA II of the synthesized metallophthalocyanine compounds **(2–4)**. The optimized 3D structures of the synthesized metallophthalocyanine compounds are presented in Fig. S13 of the supplementary material. Docking calculations reveal the interactions of synthesized metallophthalocyanine compounds with AChE, hCA I and hCA II enzymes in detail. In order to evaluate the sensitivity of the molecular docking results to the parameters, a systematic sensitivity analysis was performed on the critical parameters. In this context, variables such as grid box sizes (with ±5 Å increments in the X, Y, Z axes), exhaustiveness value (from 8 to 24), and grid spacing (from 0.375 Å to 0.6 Å) were optimized. Specifically, in the re-docking study of Tacrin for AChE and also Acetazolamide for hCA II, when the exhaustiveness value was set as 24 and the grid spacing as 0.375 Å, the RMSD value decreased from 2.04 Å to 1.89 Å. However, for large and inflexible phthalocyanine derivatives, a wider grid box ($80 \times 80 \times 80$ Å^3) and higher exhaustiveness (16) values were required. While these optimizations increased the repositioning accuracy for standard compounds, a complete match to the crystallographic conformations was not achieved due to the rigidity of the protein structure. In this context, it was noted that the rigid docking approach used has several fundamental limitations. First, the failure to account for protein flexibility can limit the accuracy of ligand binding, particularly in dynamic regions such as the catalytic triad of AChE (Ser203-His447-Glu334). Furthermore, the failure to include solvation and entropic effects in the models can lead to inadequate prediction of hydrophobic surface interactions of phthalocyanines, especially in aqueous environments. These limitations are among the main reasons for the high RMSD values (>2 Å) obtained in the redocking processes. Furthermore, the binding energies and interaction motifs of the phthalocyanine derivatives are in high agreement with experimental enzyme inhibition data (Table 2). This supports the qualitative validity of the docking approach used and the biological relevance of the results.

Table 3 The binding energy and root-mean-square deviation (RMSD) values of the metallophthalocyanine compounds **(2**, **3** and **4)**, Tacrine (TAC) for AChE; and also Acetazolamide (AZA) for hCA I and hCA II as reference compounds

AChE	Binding energy (kcal/mol)	RMSD (Å)
2	-23.29	0.870
3	-9.49	1.460
4	-26.96	1.690
Tacrine (TAC)	-7.37	1.890
hCA I	Binding energy (kcal/mol)	RMSD (Å)
2	-11.98	1.890
3	-13.90	0.940
4	-13.50	0.900
Acetazolamide (AZA)	-6.14	1.768
hCA II	Binding energy (kcal/mol)	RMSD (Å)
2	-13.51	1.330
3	-15.39	1.460
4	-12.48	1.190
Acetazolamide (AZA)	-6.56	1.890

In the docking study, as a result of the interactions of the relevant metallophthalocyanine compounds **(2–4)** with the selected targets, the best binding affinity with AChE is compound **(4)**, which shows −26.96 kcal/mol. Then, compound **(2)** with the binding energy of −23.29 kcal/mol and compound **(3)** with the binding energy of −9.49 kcal/mol interact with the target at Table 3.

These situations are displayed as the 3D orientation and residue interactions of the metallophthalocyanine compounds in the active site of AChE enzyme in Fig. 6. In addition, the binding modes of the active compounds were compared by superimposed with the reference compound, *tacrine*. This comparison provides an important reference in understanding the types of interaction of the compounds with the enzyme and evaluating their activities. Compound **(4)** containing In metal in its structure forms non-bonding interactions with AChE enzyme including hydrogen bond

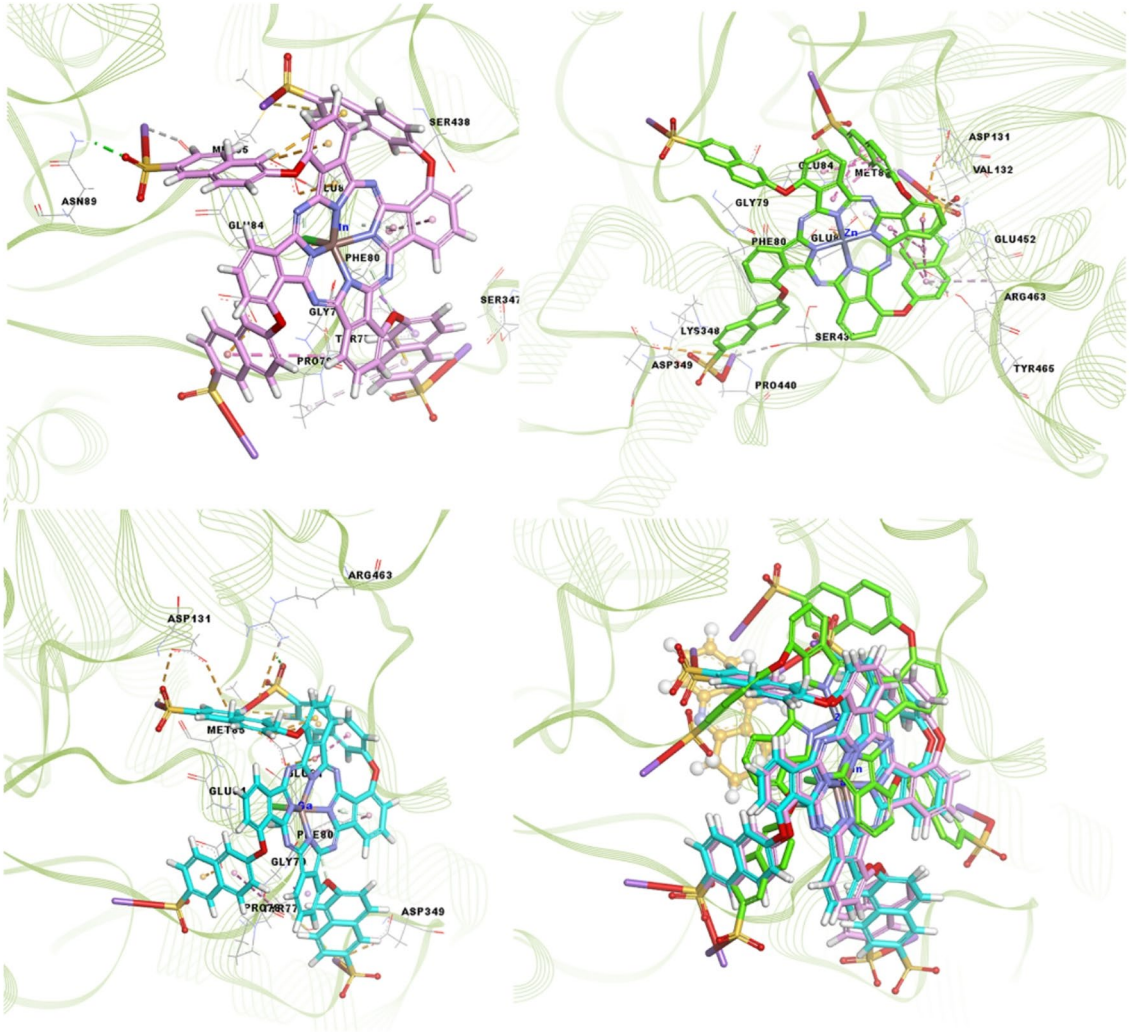


Fig. 6 3D orientation and non-bonding interactions of compounds **(4)**, **(2)** and **(3)** (shown in pink, green and blue color, stick form, respectively) interacting with active amino acids in the binding site of AChE, as well as compared Tacrine (TAC, orange color, ball and stick form)

(Asn89, Tyr77, Phe80 and Glu81), metal-acceptor (Met85), electrostatic interaction (Glu81), pi-sulfur (Met85 and Tyr77) and hydrophobic interactions (Phe80, Pro78 and Gly79). Compound **(2)** containing Zn metal shows a tendency to have electrostatic interactions (Arg463, Asp349, Glu81, Asp131 and Glu452) with different orientations and modes with the same target, with less hydrogen bond (Val132 and Tyr465), metal acceptor (Ser438 and Met85) and hydrophobic interactions (Arg463 and Met85). Finally, Compound **(3)** containing Ga metal exhibited an interaction with the target enzyme predominantly consisting of electrostatic interactions like compound **(2)**. In addition, the compound formed 3 hydrogen bonds with Arg463, Phe80 and Glu81 residues of the target. It also formed pi-sulfur bonds with Met85 and Tyr77amino acids and hydrophobic interactions with Phe80, Pro78 and Gly79. These three different metal complex structures that showed activity, due to their chemical structure diversity and topologically larger surface area than the standard compound Tacrine of the target AChE, they occured remarkable high biological activity with the target. Especially, it is observed that the compound **(4)** containing In metal is the most effective structure with numerical and molecular interactions. The interactions of the reference compound with the target enzyme are presented in detail in Fig. S14-S17 and Table S1 in the supplementary file.

When the activities of the same compounds on the second target model hCA I are evaluated, molecular docking results show that compound **(3)** is the most effective structure for this target, with a binding energy value of -13.90 kcal/mol. When the 3D orientation and interactions are examined in Fig. 7, compound **(3)** containing Ga metal creates a high binding and consequently a high binding tendency by making numerous electrostatic, hydrogen bonding,

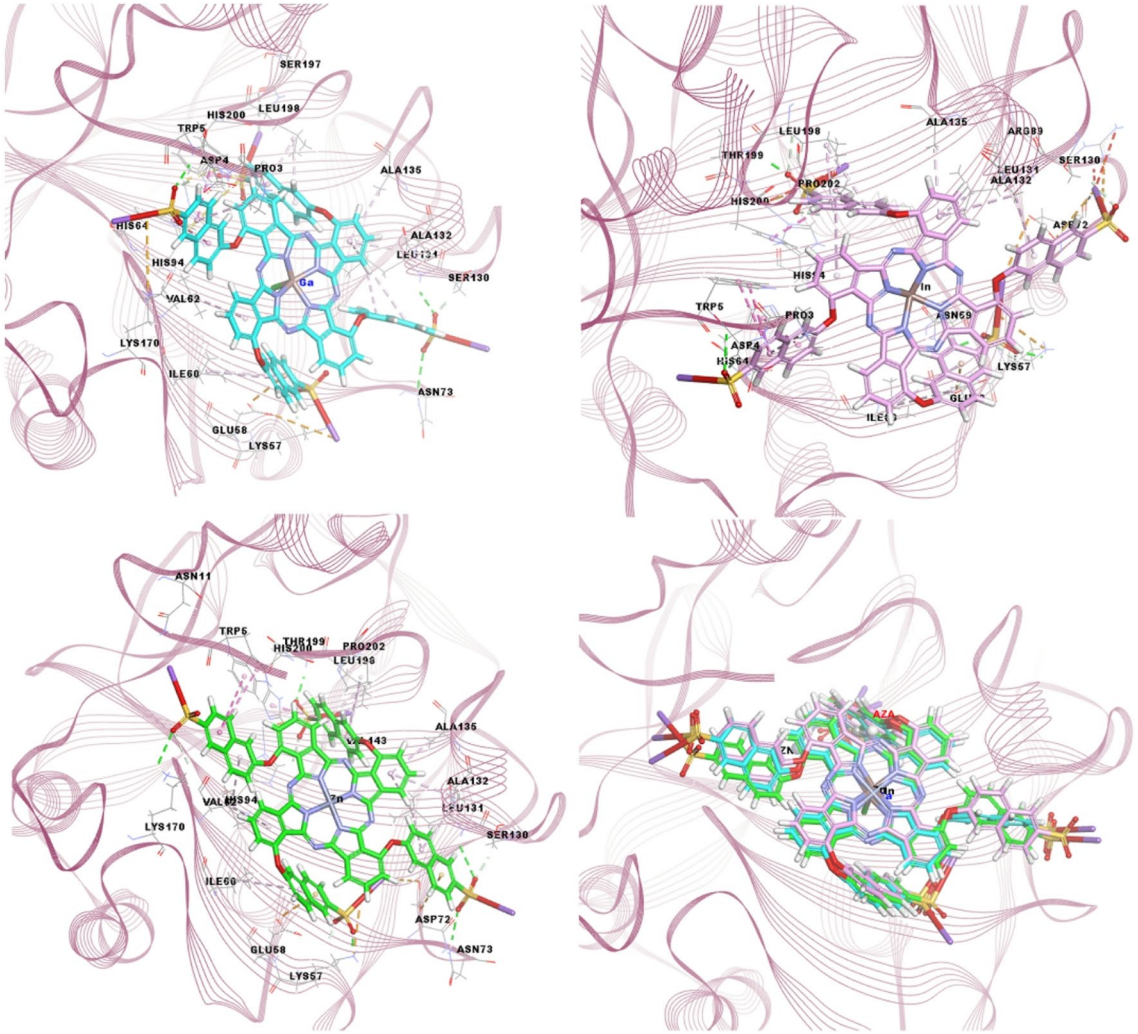


Fig. 7 3D orientation and non-bonding interactions of compounds **(3)**, **(4)** and **(2)** (shown in blue, pink, and green color, stick form, respectively) interacting with active amino acids in the binding site of hCA I, as well as compared Acetazolamide (AZA, default color, ball and stick form)

metal-acceptor, pi-sulfur and hydrophobic interactions with the target structure due to its large surface area. Then, compound **(4)** interacted with the target in a similar mode with a binding energy value of -13.50 kcal/mol, but showed a weaker activity than compound **(3)** with hCA I due to the difference in metals between them. Compound **(2)** shows a binding energy value of -11.98 kcal/mol with the same target due to the difference in orientation and the Zn metal in its structure.

Finally, the metallophthalocyanine complexes are examined against hCA II. The potent structure is compound **(3)** as in hCA I. However, the relevant compound has a binding value of -15.39 kcal/mol with hCA II, which binds better than hCA (I) This is because the active site of hCA II is larger than that of hCA I and the non-binding interactions are stronger than the others. In the second place, compound **(2)** interacts with the target structure with a binding affinity of -13.51 kcal/mol. Then, compound **(4)**, that is, the structure containing In metal, shows a binding affinity of -12.48 kcal/mol with the target enzyme. As a reason for this, we can state the different orientations and metal differences in the active site of the target enzyme hCA (II) In addition, these situations are presented visually in Fig. 8 and in the additional file as Table 3.

The results of this part reveal that the biological activities of metallophthalocyanine complexes may vary significantly depending on the type of metal to which they are bound. In particular, compound **(4)** containing Indium (In) metal was found to have a strong inhibitory effect on the acetylcholinesterase (AChE) enzyme. This suggests that compound **(4)** may be a potential candidate in the treatment of neurodegenerative diseases. On the other hand, compound **(3)** containing Gallium (Ga) metal was found to have a potential inhibitory activity on human carbonic anhydrase I and II

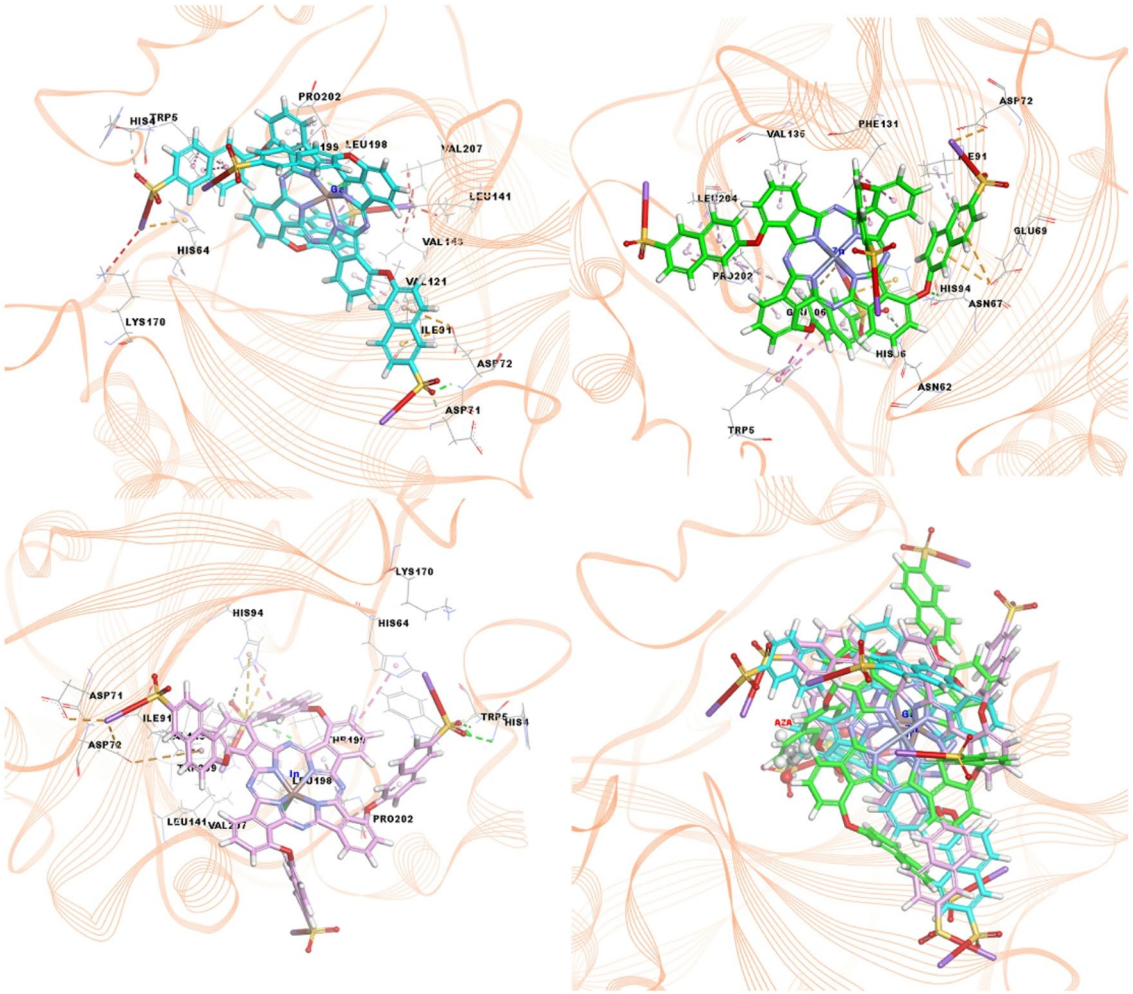


Fig. 8 3D orientation and non-bonding interactions of compounds **(3)**, **(2)** and **(4)** (shown in blue, green, and pink color, stick form, respectively) interacting with active amino acids in the binding site of hCA II, as well as compared Acetazolamide (AZA, default color, ball and stick form)

(hCA I and hCA II) enzymes. This indicates that compound **(3)** may be used in the treatment of diseases in which carbonic anhydrase enzymes play a role, especially glaucoma and cancer.

3 Conclusion

This study reports the preparation of a new ligand, *sodium 6-(2,3-dicyanophenoxy)naphthalene-2-sulfonate* **(1)**, and its corresponding non-peripherally substituted metallophthalocyanines containing zinc(II) **(2)**, gallium(III) chloride **(3)**, and indium(III) chloride **(4)** by featuring "*6-naphthoxy-2-sulfonic acid sodium salt*" units at their non-peripheral positions. Compounds **(2–4)** were investigated for photochemical and sonophotochemical applications in both DMSO and H_2O. In such applications singlet oxygen production capacity are very important. To evaluate the compounds' capacity both light and ultrasound+light were employed as sensitizing agent. The collected datas show that all compounds **(2–4)** have greater singlet oxygen generation than std-ZnPc in photochemical method. In addition, by changing the stimulating method to ultrasound+light, the singlet oxygen production of the compounds was further increased. We conducted in vitro and in silico studies on these new complexes and the results were significant and we determined their anti-epileptic and anti-AD properties and these complexes are suitable for future in vivo studies and can be examples for drug design. Compound **(4)** containing Indium (In) stands out as a strong inhibitor for AChE, while compound **(3)** containing Gallium (Ga) shows potential activity on hCA I and hCA II enzymes. These findings reveal that the biological activity of metallophthalocyanine compounds varies depending on the metal type. Overall, the synthesized water-soluble metallophthalocyanines **(2–4)** exhibited measurable inhibitory effects on AChE and hCA isoenzymes, as well as promising results in terms of photo- and sonophoto-induced singlet oxygen production. These

findings should be considered primarily as evidence of biochemical interaction potential, rather than as an indication of direct pharmacological applicability. The combination of enzyme-targeting ability and photodynamic reactivity suggests that these complexes could serve as key molecules for the future development of multifunctional imaging or therapeutic systems, particularly where oxidative or enzymatic pathways are involved.

Supplementary Information The online version contains supplementary material available at https://doi.org/10.1007/s43630-026-00866-4.

Acknowledgements The numerical calculations reported in this paper were partially performed at TUBITAK ULAKBIM, High Performance and Grid Computing Center (TRUBA resources).

Author contributions I Prof. Armağan GÜNSEL hereby declare that all the authors agree to submit the paper to Photochemical & Photobiological Sciences and agreeing with the authorship as well.

Funding Open access funding provided by the Scientific and Technological Research Council of Türkiye (TÜBİTAK).

Data availability The authors declare that the data supporting the findings of this study are available within the paper and its Supplementary Information file.

Declarations

Conflict of interest The authors declare no conflict of interest.

Open Access This article is licensed under a Creative Commons Attribution 4.0 International License, which permits use, sharing, adaptation, distribution and reproduction in any medium or format, as long as you give appropriate credit to the original author(s) and the source, provide a link to the Creative Commons licence, and indicate if changes were made. The images or other third party material in this article are included in the article's Creative Commons licence, unless indicated otherwise in a credit line to the material. If material is not included in the article's Creative Commons licence and your intended use is not permitted by statutory regulation or exceeds the permitted use, you will need to obtain permission directly from the copyright holder. To view a copy of this licence, visit http://creativecommons.org/licenses/by/4.0/.

References

1. McKeown, N. B. (1998). *Phthalocyanine materials: synthesis, structure and function*. Cambridge University Press.
2. Li, X., Zheng, B. D., Peng, X. H., Li, S. Z., Ying, J. W., Zhao, Y., Huang, J. D., & Yoon, J. (2019). Phthalocyanines as medicinal photosensitizers: Developments in the last five years. *Coordination Chemistry Reviews*, *379*, 147–160.
3. Aggarwal, A., Samaroo, D., Jovanovic, I. R., Singh, S., Tuz, M. P., & Mackiewicz, M. R. (2019). Porphyrinoid-based photosensitizers for diagnostic and therapeutic applications: An update. *J Porphyrins Phthalocyanines*, *23*, 729–765.
4. Zhao, J. F., Wang, J., Chen, J. Y., Chidawanykia, W., Nyokong, T., Ishii, K., & Kobayashi, N. (2012). Gallium phthalocyanine photosensitizers: Carboxylation enhances the cellular uptake and improves the photodynamic therapy of cancers. *ACAMC*, *12*, 604–610.
5. Rosenthal, I., & PHTHALOCYANINES AS PHOTODYNAMIC SENSITIZERS*. (1991). *Photochem & Photobiology*, 53, 859–870.
6. Durmuş, M., & Nyokong, T. (2007). Synthesis, photophysical and photochemical properties of aryloxy tetra-substituted gallium and indium phthalocyanine derivatives. *Tetrahedron*, *63*, 1385–1394.
7. Macdonald, I. J., & Dougherty, T. J. (2001). Basic principles of photodynamic therapy. *J Porphyrins Phthalocyanines*, *05*, 105–129.
8. Günsel, A., Kocabaş, S., Bilgiçli, A. T., Güney, S., & Kandaz, M. (2016). Synthesis, photophysical and electrochemical properties of water–soluble phthalocyanines bearing 8-hydroxyquinoline-5-sulfonicacid derivatives. *Journal of Luminescence*, *176*, 387–396.
9. Van De Winckel, E., Mascaraque, M., Zamarrón, A., De La Fuente, Á. J., & Torres, T. (2018). De La Escosura, dual role of subphthalocyanine dyes for optical imaging and therapy of cancer. *Adv Funct Materials*, *28*, 1705938.
10. Cheng, D., Wang, X., Zhou, X., & Li, J. (2021). Nanosonosensitizers with ultrasound-induced reactive oxygen species generation for cancer sonodynamic immunotherapy. *Frontiers in Bioengineering and Biotechnology*, *9*, 761218.
11. Günsel, A., Küçük, M. C., Günsel, H., Yaşa Atmaca, G., Bilgiçli, A. T., Erdoğmuş, A., & Yarasir, M. N. (2023). 3-Chloro-4-fluorophenoxy substituted zinc phthalocyanine/graphene oxide composites: Exploring of their sono-photochemical properties. *Chemical Papers*, *77*, 5721–5731.
12. Karanlık, C. C., Atmaca, G. Y., & Erdoğmuş, A. (2021). Improved singlet oxygen yields of new palladium phthalocyanines using sonochemistry and comparisons with photochemistry. *Polyhedron*, *206*, 115351.
13. Günsel, A., Mutlu, N., Yaşa Atmaca, G., Günsel, H., Bilgiçli, A. T., & Erdoğmuş, A. (2023). and M. Nilüfer Yarasir, Novel Graphene Oxide/Zinc Phthalocyanine Composites Bearing 3-Chloro-4-Fluorophenoxy: Potential Usage for Sono/Photochemical Applications, *ChemistrySelect*, 8, e202204546.
14. Tunca, H., Özpinar, S. Ç., TEKBABA, A. G., Sevindik, T. O., & GÜNSEL, A. (2022). BİLGİÇLİ and M. N. YARAŞIR, algaecidal and oxidative effects of metal-free phthalocyanine beta tetra-substituted with sodium 2-mercaptoethanesulfonate. *Turkish Journal of Chemistry*, *46*, 367–377.
15. Lo, P. C., Rodríguez-Morgade, M. S., Pandey, R. K., Ng, D. K., Torres, T., & Dumoulin, F. (2020). The unique features and promises of phthalocyanines as advanced photosensitisers for photodynamic therapy of cancer. *Chemical Society Reviews*, *49*, 1041–1056.
16. Al-Hamdan, N. S., Hussain, A., Kozlikova, M., Alfred, M. A., Machacek, M., Ganesan, A., Zimcik, P., & Makhseed, S. (2024). Enhanced photodynamic activity of asymmetric non-ionic Zn (II) phthalocyanine amphiphiles: Effect of molecular design on in vitro activity. *Dyes and Pigments*, *221*, 111809.
17. Zhao, Y., Zhang, X., Chen, Z., Xu, Y., Kim, H., Jeong, H., Lee, Y. R., Lee, J., Li, X., & Yoon, J. (2024). Supramolecular phthalocyanine assemblies-enhanced synergistic photodynamic and photothermal therapy guided by photoacoustic imaging. *Aggregate*, *5*, e514.
18. Mahmudov, I., Ibrahimova, B., Taslimi, P., Sadeghian, N., Karaoğlan, Z., Taskin-Tok, T., Abdullayev, Y., Farzaliyev, V., Sujayev, A., & Alwasel, S. H. (2024). Synthesis, characterization, crystal structure, molecular docking, and biological studies of Cu, Ni and Co metal complexes of pyrazole. *Journal of Molecular Structure*, *1309*, 138205.

19. Tapera, M., Kekeçmuhammed, H., Tüzün, B., Daştan, S. D., Çelik, M. S., Taslimi, P., Dastan, T., Topcu, K. S. B., Cacan, E., & Şahin, O. (2024). Novel 1, 2, 4-triazole-maleamic acid derivatives: Synthesis and evaluation as anticancer agents with carbonic anhydrase inhibitory activity. *Journal of Molecular Structure*, *1313*, 138680.
20. Medetalibeyoğlu, H., Manap, S., Alkan, M., Beytur, M., Barlak, N., Karatas, O. F., Tüzün, B., Yüksek, H., Taslimi, P., Novel Schiff Bases: Synthesis, Characterization, Bioactivity, Cytotoxicity, and, & Evaluations, C. (2024). *Polycyclic Aromatic Compounds*, 1–19.
21. Durmaz, L., Karageçili, H., Erturk, A., Ozden, E. M., Taslimi, P., Alwasel, S., & Gülçin, İ. (2024). Hamamelitannin's antioxidant effect and its Inhibition capability on α-glycosidase, carbonic anhydrase, acetylcholinesterase, and butyrylcholinesterase enzymes. *Processes*, *12*, 2341.
22. Fatullayeva, P. A., Medjidov, A. A., Safronenko, M. G., Khrustalev, V. N., Ismayilov, R. H., Bayramov, M. A., Yalcin, B., Sadeghian, N., Taslimi, P., & Tuzun, B. (2024). Bioactivity, crystal and molecular structure of Vanadyl (III) complex with N-salicyloyl-N'(3, 5-ditertbutyl-2-hydroxy) benzylidene hydrazine. *Polyhedron*, *257*, 117024.
23. Solğun, D. G., Sadeghian, N., Taskin-Tok, T., Ağirtaş, M. S., & Taslimi, P. (2024). Synthesis, fluorescence, enzymes effects, and evaluation of tetrahydroxy substituted zinc phthalocyanine as multitarget metabolic enzyme inhibitors with molecular docking: The biochemistry-oriented drug design. *J IRAN CHEM SOC*, *21*, 2413–2424.
24. Alishba, I., Ali, S., Hameed, K. M., Khan, U., Salar, M., Taha, N., Sadeghian, P., Taslimi, B., Tuzun, D., Özerkan, H., Dedeakayogullari, & Ulukaya, E. (2024). Exploring Benzo[*b*][1,4] Thiazine Derivatives: Multitarget Inhibition, Structure–Activity Relationship, Molecular Docking, and ADMET Analysis, *ChemistrySelect*, 9, e202404087.
25. Abbasova, G., Medjidov, A., Ismayilov, R., Tagiyev, D., Sertçelik, M., Hökelek, T., Huseynova, M., Fatullaeva, P., Çakır, F., & Şenol, H. (2025). Photoorganocatalytic synthesis, characterization, crystal structure of two schiff bases and their in vitro and in Silico evaluations as cholinesterase inhibitors. *Journal of Molecular Structure*, *1329*, 141396.
26. Ol'ga, V. P., Tomilin, D. N., Şenol, H., Belyaeva, K. V., Nikitina, L. P., Oparina, L. A., Sobenina, L. N., Trofimov, B. A., Sadeghian, N., & Taslimi, P. (2024). Synthesis of pyrrole-heterocyclic derivatives as anti-Alzheimer and antidiabetic candidates: An in vitro-in Silico study. *Journal of Molecular Structure*, *1315*, 138998.
27. Yalazan, H., Koç, D., Aydın Kose, F., Fandaklı, S., Tüzün, B., Akgül, M. İ., Sadeghian, N., Taslimi, P., & Kantekin, H. (2023). Design, syntheses, theoretical calculations, MM-GBSA, potential anti-cancer and enzyme activities of novel schiff base compounds. *Journal of Biomolecular Structure and Dynamics*, 1–14.
28. Günsel, A., Yıldırım, A., Taslimi, P., Erden, Y., Taskin-Tok, T., Pişkin, H., Bilgicli, A. T., Gülçin, İ., & Yarasir, M. N. (2022). Cytotoxicity effects and biochemical investigation of novel tetrakis-phthalocyanines bearing 2-thiocytosine moieties with molecular Docking studies. *Inorganic Chemistry Communications*, *138*, 109263.
29. Çamur, M., Durmuş, M., & Bulut, M. (2011). Synthesis, characterization and comparative studies on the photophysical and photochemical properties of metal-free and zinc (II) phthalocyanines with phenyloxyacetic acid functionalities. *Polyhedron*, *30*, 1935–1944.
30. Khene, S., Ogunsipe, A., Antunes, E., & Nyokong, T. (2007). Microwave synthesis and photophysics of new tetrasulfonated tin(II) macrocycles. *J Porphyrins Phthalocyanines*, *11*, 109–117.
31. Durmuş, M., & Nyokong, T. (2007). Synthesis, photophysical and photochemical studies of new water-soluble indium(iii) phthalocyanines. *Photochemical & Photobiological Sciences*, *6*, 659–668.
32. Gaspard, S., & Maillard, P. (1987). Structure des Phtalocyanines tetra tertio-butylees: Mecanisme de La synthese. *Tetrahedron*, *43*, 1083–1090.
33. Mack, J., & Kobayashi, N. (2011). Low symmetry phthalocyanines and their analogues. *Chemical Reviews*, *111*, 281–321.
34. Bilgiçli, A. T., Günsel, A., Kandaz, M., & Özkaya, A. R. (2012). Highly selective thioalcohol modified phthalocyanine sensors for ag (I) and Pd (II) based on target induced J-and H-type aggregations: synthesis, electrochemistry and peripheral metal ion binding studies. *Dalton Transactions*, *41*, 7047–7056.
35. Günsel, A., Bilgiçli, A. T., Kandaz, M., Orman, E. B., & Özkaya, A. R. (2014). Ag (I) and Pd (II) sensing, H-or J-aggregation and redox properties of metal-free, Manganase (III) and gallium (III) phthalocyanines. *Dyes and Pigments*, *102*, 169–179.
36. Göksel, M., Durmuş, M., & Atilla, D. (2012). A comparative study on photophysical and photochemical properties of zinc phthalocyanines with different molecular symmetries. *J Porphyrins Phthalocyanines*, *16*, 895–906.
37. Ogunsipe, A., Maree, D., & Nyokong, T. (2003). Solvent effects on the photochemical and fluorescence properties of zinc phthalocyanine derivatives. *Journal of Molecular Structure*, *650*, 131–140.
38. Bıyıklıoğlu, Z., Durmuş, M., & Kantekin, H. (2011). Tetra-2-[2-(dimethylamino) ethoxy] ethoxy substituted zinc phthalocyanines and their quaternized analoques: synthesis, characterization, photophysical and photochemical properties. *Journal of Photochemistry and Photobiology A: Chemistry*, *222*, 87–96.
39. Ng, A. C. H., Li, X., & Ng, D. K. P. (1999). Synthesis and photophysical properties of nonaggregated phthalocyanines bearing dendritic substituents. *Macromolecules*, *32*, 5292–5298.
40. Günsel, A., Kandaz, M., Koca, A., & Salih, B. (2011). Peripheral and non-peripheral-designed multifunctional phthalocyanines; synthesis, electrochemistry, spectroelectrochemistry and metal ion binding studies. *Polyhedron*, *30*, 1446–1455.
41. Ogunsipe, A., & Nyokong, T. (2005). Photophysical and photochemical studies of sulphonated non-transition metal phthalocyanines in aqueous and non-aqueous media. *Journal of Photochemistry and Photobiology A: Chemistry*, *173*, 211–220.
42. Schnurpfeil, G., Sobbi, A. K., Spiller, W., Kliesch, H., & Wöhrle, D. (1997). Photo-oxidative stability and its correlation with Semiempirical MO calculations of various tetraazaporphyrin derivatives in solution. *J Porphyrins Phthalocyanines*, *01*, 159–167.
43. Karanlık, C. C., Karanlık, G., & Erdoğmuş, A. (2023). Water-soluble meso-thienyl BODIPY therapeutics: Synthesis, characterization, exploring photophysicochemical and DNA/BSA binding properties. *Journal of Photochemistry and Photobiology A: Chemistry*, *438*, 114581.
44. Turkkol, A., Can Karanlık, C., Calıskan, S. G., Bilgin, M. D., Erdoğmuş, A., & Güzel, E. (2024). Hybrid Sono-Photodynamic combination therapy mediated by Water-Soluble gallium phthalocyanine enhances the cytotoxic effect against breast cancer cell lines. *ACS Appl Bio Mater*, *7*, 2725–2733.
45. Günsel, A., Bilgiçli, A. T., Kırbaç, E., Güney, S., & Kandaz, M. (2015). Water soluble quarternizable gallium and indium phthalocyanines bearing Quinoline 5-sulfonic acid: Synthesis, aggregation, photophysical and electrochemical studies. *Journal of Photochemistry and Photobiology A: Chemistry*, *310*, 155–164.
46. Dilber, G., Durmuş, M., & Kantekin, H. (2019). Non-aggregated zwitterionic zinc (II) phthalocyanine complexes in water with high singlet oxygen quantum yield. *Dyes and Pigments*, *160*, 267–284.
47. Galstyan, A., & Dobrindt, U. (2018). Breaching the wall: Morphological control of efficacy of phthalocyanine-based photoantimicrobials. *Journal of Materials Chemistry B*, *6*, 4630–4637.

48. İ, Ömeroğlu, & Durmuş, M. (2023). Water-soluble phthalocyanine photosensitizers for photodynamic therapy. *Turkish Journal of Chemistry*, *47*, 837–863.
49. Ozcan, I., Alici, H., Taslimi, P., & Tahtaci, H. (2025). Novel 1, 2, 4-triazole-derived schiff base derivatives: Design, synthesis, and multi-enzyme targeting potential for therapeutic applications. *Bioorganic Chemistry*, 108246.
50. Akkus, M., Kirici, M., Poustforoosh, A., Erdogan, M. K., Gundogdu, R., Tüzün, B., & Taslimi, P. (2025). Phenolic compounds: Investigating their Anti-Carbonic Anhydrase, Anti-Cholinesterase, Anticancer, Anticholinergic, and antiepileptic properties through molecular Docking, MM-GBSA, and dynamics analyses. *Korean Journal of Chemical Engineering*, *42*, 1149–1168.
51. Güzel, E., Arslan, B. S., Çıkrıkçı, K., Ergün, A., Gençer, N., Arslan, O., Şişman, İ., & Nebioğlu, M. (2020). Synthesis, *in vitro* inhibition effect of novel phthalocyanine complexes as carbonic anhydrase and paraoxonase enzyme inhibitors, *J. Porphyrins Phthalocyanines*, 24, 1047–1053.
52. Çakır, V., & Arslan, T. (2022). Synthesis and biological evaluation of new silicon (IV) phthalocyanines as carbonic anhydrase and cholinesterase inhibitors. *Inorganica Chimica Acta*, *530*, 120678.
53. Farzaliyeva, A., Şenol, H., Taslimi, P., Çakır, F., Farzaliyev, V., Sadeghian, N., Mamedov, I., Sujayev, A., Maharramov, A., & Alwasel, S. (2025). Synthesis and biological studies of acetophenone-based novel chalcone, semicarbazone, thiosemicarbazone and Indolone derivatives: Structure-Activity relationship, molecular docking, molecular dynamics, and kinetic studies. *Journal of Molecular Structure*, *1321*, 140197.
54. Güzel, E., Koçyiğit, Ü. M., Taslimi, P., Gülçin, İ., Erkan, S., Nebioğlu, M., Arslan, B. S., & Şişman, İ. (2022). Phthalocyanine complexes with (4-isopropylbenzyl)oxy substituents: Preparation and evaluation of anti-carbonic anhydrase, anticholinesterase enzymes and molecular Docking studies. *Journal of Biomolecular Structure and Dynamics*, *40*, 733–741.
55. Tekin, A., & Arslan, T. (2022). Investigation of cholinesterase inhibitor effects of some chalcone substituted metallophthalocyanines. *Karadeniz Fen Bilimleri Dergisi*, *12*, 703–711.